THESIS FOR THE DEGREE OF LICENTIATE OF PHILOSOPHY

Numerical modelling of time-dependent metamaterials with the FDTD method

SERGEY NOVOZHILOV

Department of Physics
CHALMERS UNIVERSITY OF TECHNOLOGY
Göteborg, Sweden 2018

Numerical modelling of time-dependent metamaterials with the FDTD method
SERGEY NOVOZHILOV

Department of Physics
Chalmers University of Technology
SE-412 96 Göteborg
Sweden
Telephone: +46 (0)31-772 1000

Chalmers Reproservice
Göteborg, Sweden 2018

Numerical modelling of time-dependent metamaterials with the FDTD method
SERGEY NOVOZHILOV
Department of Physics
Chalmers University of Technology

Abstract

Metamaterials are artificial materials, usually composed of so-called meta-atoms, with electromagnetic properties which cannot be found in naturally occurring materials. In this work we study the properties of time-dependent metamaterials (meaning that their electromagnetic properties are varying with time), as well as their potential applications. Since the analytical results available are limited, we have developed and implemented a numerical technique based on the Finite-Differences Time-Domain (FDTD) method. The method and its implementation are discussed in detail. A state-of-the-art variation of the total-field / scattered-field technique is used to introduce plane waves into the computational domain, so that numerical artifacts are within the limits of computing precision. We use convolutional perfectly matched layers as absorbing boundary conditions and practically demonstrate that they are well-suited for applications involving time-dependent media. Transmission of plain monochromatic waves through a time-dependent slab with the dielectric permittivity and magnetic permeability changing linearly with time, which has been investigated analytically in an earlier work, is studied numerically. Propagation of pulses with a finite continuous spectrum through the same system is studied both analytically and numerically. In all cases, the analytical and numerical results are in good agreement, which demonstrates that the code developed produces physically valid results. The technique developed is a powerful tool for designing new devices based on time-dependent metamaterials. We discuss one example of such an application, namely modelling a tunable wavelength-division multiplexer, as well as the prospects of designing other optical devices.

Keywords: FDTD, metamaterials, time-dependent media, computational electrodynamics, numerical modelling

Acknowledgements

First of all, I would like to acknowledge Philippe Tassin for suggesting the research task and the opportunity to pursue it at Chalmers. I wish to thank Thomas Ericsson, whose vision has inspired several aspects of my programs' design in general and the choice of Fortran 90 in particular for this work. I would also like to mention Sergei Tretyakov for some interesting discussions on the 'physical' and 'engineering' sides of metamaterials and some other aspects, such as the design 'paradox' of the first negative-index material, discussed in this work. I am also thankful to Stefano Maci for discussions about metasufraces and their potential applicability to this work, and to Nader Engheta for talks on various topics regarding metamaterials, including those mentioned above. I would also like to recognise that Jari Kinaret has raised in interesting discussion about the place of time-dependent models used in this work in the general picture, where the electromagnetic response is generally non-local. I am grateful to Mikael Öhman for the LaTeX template he has written for Chalmers theses and his helpful hints and suggestions for preparing a better document. And lastly, I wish to thank Leonid Gorelik: without his immense help in preparing this manuscript and his fundamental approach to even small matters, this dissertation would not be the same.

List of publications

This thesis consists of an extended introduction and the following appended paper:

Paper 1 S. Novozhilov. Numerical modelling of time-dependent metamaterials with the FDTD method (Manuscript in preparation for submission to a scientific journal)

Contents

1 Introduction

1.1 Context and objectives

When reflecting on the influx of research activities in the emerging field of metamaterials in the 21st century, one could probably name three main reasons for it: scientific curiosity, inspiring experimental successes in fabricating the samples of these novel materials, and the prospects of fabricating new devices based on optical elements, rather than conventional electronic ones. The relation between these three factors is not always trivial. For example, the so-called left-handed media had been forgotten for more than 30 years until the interest in them was rekindled due to pioneering experimental works; yet the few successful technological applications so far are related not to the left-handed optical materials per se, but to using similar ideas for engineering transmission lines. Moreover, many of the significant advances, some of which we shall discuss in the following, arise from the sharing of ideas between physics and electrical engineering in both directions. This demonstrates that the logic of the field's development is not always straightforward, and the practically useful results stemming from it are not always as initially expected.

This thesis is dedicated to time-dependent metamaterials, i.e. artificial materials with time-varying electromagnetic properties. While the existence thereof is in many ways a 'what if' matter, we believe it feasible not to limit our scientific imagination to conventional time-invariant media. The focus of this work so far is primarily not the *how*, but the *what for* question: we are mainly investigating the properties that time-dependent metamaterials would have and the subsequent applications. For this purpose, we have devised and implemented a numerical technique for modelling the properties of such materials, as well as designing optical devices based on them. Nevertheless, while we start with a macroscopic approach[1] to time-dependent metamaterials and wave phenomena occurring in them, nothing precludes from utilising the same numerical method — and the already developed programmatic code — to simulate them on a microscopic level, meaning that the parameters of microscopic 'building blocks' vary with time, so that an effective medium with desired time-dependent macroscopic properties is constructed as a result. Since both aspects are important for potential applications, we also put forth some general suggestions as to how such systems can be realised, despite the first part of the whole problem being mainly addressed to in this work.

1.2 Thesis outline

The thesis is structured as follows: in Chapter 2 a brief overview of metamaterials in general and potential implementations of time-dependent metamaterials in particular is given (for conventional time-varying media, the reader can refer to Paper 1); after that, in Chapter 3, we discuss the theoretical basics of time-dependent metamaterials first and subsequently elaborate on the numerical method developed. Finally, the manuscript of Paper 1 is attached.

[1] The hierarchy of scales is considered in more detail in Chapter 3.

2 Metamaterials: from negative refraction to generic light manipulation

While the understanding of the term 'metamaterial' has evolved somewhat, the most general modern definition comprises artificial materials with electromagnetic properties which cannot be found in naturally occurring ones. It is usually implied that metamaterials are composed of artificial subwavelength structural elements — so-called meta-atoms — so that the description in terms of continuous medium is still valid. As a result, the electromagnetic response is defined by the properties of meta-atoms, rather than atoms (some terminological nuances have been discussed in literature [1]). As opposed to the assortment of substances available in nature, these meta-atoms can be, to a degree, engineered at will. Due to this, resulting metamaterials can exhibit unusual properties, such as magnetic response at optical frequencies, negative refraction index, etc.

In this chapter, we start from a brief and somewhat historical introduction to metamaterials in general, in order to glimpse their distinct features and main design ideas. Afterwards, we focus more on tunable metamaterials in particular in the light of their applicability to engineering time-dependent metamaterials, which we are primarily interested in in the context of this work.

2.1 The concept of left-handed materials

In the beginning, metamaterials were all but synonymous to so-called negative-index, or left-handed, materials. A comprehensive theoretical review of negative-index media, as well as their associated properties, by Veselago [2] has received the most recognition. However, both negative refraction itself [3] (fig. 2.1) and its relation to media with simultaneously negative dielectric permittivity ϵ and magnetic permeability μ [4, 5], had also been studied earlier.

It is remarkable that the theoretical possibility of negative refraction was conceived as early as in 1944 in Mandelshtam's lectures (published afterwards as a book [3]) — even before the material properties required were investigated. He does not address material parameters specific to optical waves, such as the dielectric permittivity or the refractive index, directly. Instead, he operates with very general concepts such as boundary conditions, phase and group velocity, energy flow, which are universal for various types of waves. Let us consider this approach to negative refraction, following Mandelshtam's exposition.

In order to study reflection and refraction of waves on an infinite plane surface $y = 0$ separating two different isotropic media at $y > 0$ and $y < 0$ (fig. 2.2), one considers the following plane monochromatic waves with the frequency ω: the incident wave at $y < 0$ with the wavevector

$$\mathbf{k}_i = k(\omega)(\mathbf{e}_x \sin(\varphi) + \mathbf{e}_y \cos(\varphi)) \tag{2.1}$$

and a unit amplitude, the reflected wave at $y < 0$ with the wavevector

$$\mathbf{k}_r = k(\omega)(\mathbf{e}_x \sin(\varphi') - \mathbf{e}_y \cos(\varphi')) \tag{2.2}$$

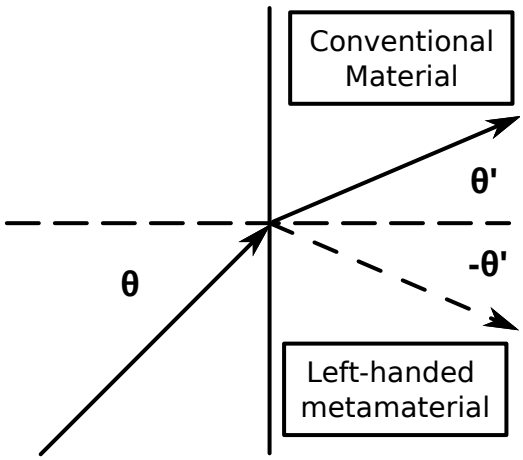

Figure 2.1: *Positive and negative refraction in conventional and negative-index materials.*

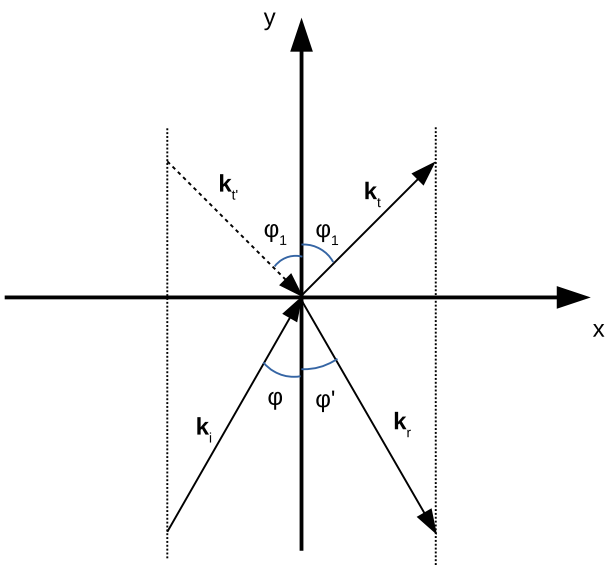

Figure 2.2: *Four possible waves at the boundary ($y = 0$) between two media. The one shown with dashed line, propagating towards the boundary, is discarded for conventional Fresnel conditions.*

and the complex amplitude R and the refracted wave at $y > 0$ with the wavevector

$$\mathbf{k}_t = k_1(\omega)(\mathbf{e}_x \sin(\varphi_1) + \mathbf{e}_y \cos(\varphi_1)) \tag{2.3}$$

and the complex amplitude T, where $k(\omega), k_1(\omega)$ are the respective wavenumbers, derived from the dispersion relation in each medium. E.g. for optical waves, we can assume for simplicity that the light falls from vacuum, and $k = \omega/c$.

At the plane $y = 0$, these waves must satisfy the boundary conditions. For example, in elastic bodies this means that the stresses and displacements must be continuous across the boundary. For an electromagnetic problem, the normal components of $\mathbf{D}$ and $\mathbf{B}$ and the tangential components of $\mathbf{E}$ and $\mathbf{H}$ must satisfy the same requirement. One can demonstrate that the boundary conditions are generally impossible to satisfy with only the reflected or refracted wave[1], while with both of these waves present, there exists a unique solution to the boundary problem (indeed, the boundary conditions result in two linearly independent equations for two normalised complex field amplitudes R and T as unknown variables). Mathematically, however, this is not the most general solution: another wave at $y > 0$ with the wavevector

$$\mathbf{k}_{t'}(\varphi_1) = \mathbf{k}_t(\pi - \varphi_1) = k_1(\omega)(\mathbf{e}_x \sin(\varphi_1) - \mathbf{e}_y \cos(\varphi_1)) \tag{2.4}$$

and the amplitude T' is also compatible with the boundary conditions. Conventionally, though, it is assumed that this wave is absent. We shall see its role in the following.

From the boundary conditions, one can derive the laws of reflection

$$\sin\varphi = \sin\varphi', \text{or } \varphi = \varphi', \tag{2.5}$$

and refraction (Snell's law):

$$k \sin\varphi = k_1 \sin\varphi_1. \tag{2.6}$$

We should note that eqs. (2.5) and (2.6) are universal for waves of different nature for a clear physical reason: they essentially mean that due to translational symmetry, the k_x component of the wavevector is continuous across the boundary.

Equation (2.6) can be satisfied for both wavevectors $\mathbf{k}_t(\varphi_1)$ and $\mathbf{k}_{t'}(\varphi_1)$, with the first wave propagating away from the boundary, and the second one — towards it. The latter contradicts the intuitive picture of the refracted wave propagating away from the boundary, therefore this wave is usually discarded, as we have noted previously. However, the direction where the *phase* flows, i.e. the direction of the wavevector, does not necessarily coincide with the direction of the *energy* flow. The latter is of great physical importance, since for the refraction problem in question, the energy should always flow outwards, i.e. away from the boundary. Matter of fact, for a variety of physical systems supporting wave propagation, the energy velocity is equal not to the *phase velocity*, but to the *group velocity* — should the latter be well-defined[2]. If the phase and group velocities

[1] Obviously, the general case is meant here. For certain particular cases, e.g. normal incidence on an impedance-matched medium or total internal reflection, the amplitudes of reflected or transmitted waves can be zero.

[2] The group velocity is defined as the speed of the slowly varying envelope. In this case, it can be calculated as $\partial\omega/\partial\mathbf{k}$. If the envelope is not varying slowly, then the group velocity is not well-defined.

have opposite directions, then the phase must flow *towards* the boundary, resulting in refraction at a negative angle. This corresponds with the fourth wave, discarded in the conventional derivation of Fresnel's conditions.

While the reasoning above is very general and pertinent to waves regardless of their nature, the connection between negative refraction of electromagnetic radiation and simultaneously negative dielectric permittivity ϵ and magnetic permeability μ (thus dubbed also double-negative) in particular has been noted by Sivukhin [4] and considered more thoroughly by Pafomov [5]. Finally, Veselago provided a comprehensive theoretical review of such materials. Let us consider the relation between the phase velocity, the direction of energy flow and the material properties for electromagnetic waves and thus explore also the possibilities for negative refraction.

Electromagnetic field in continuous media can be characterised by four vector fields: the electric field $\mathbf{E}$, the electric induction $\mathbf{D}$, the magnetic induction $\mathbf{B}$ and the magnetic field $\mathbf{H}$. For plain monochromatic waves in a linear, isotropic medium with the dielectric permittivity $\epsilon(\omega)$ and magnetic permeability $\mu(\omega)$ (as we shall see, the role of frequency dispersion is essential; we shall, however, neglect the spatial dispersion), the fields $\mathbf{E}$, $\mathbf{D}$, $\mathbf{B}$ and $\mathbf{H}$ have the following form:

$$\mathbf{E}(\mathbf{r},t) = \frac{1}{2}\mathbf{E_0}\exp(i(\mathbf{kr}-\omega t)) + \text{c.c.}, \tag{2.7}$$

$$\mathbf{H}(\mathbf{r},t) = \frac{1}{2}\mathbf{H_0}\exp(i(\mathbf{kr}-\omega t)) + \text{c.c.}, \tag{2.8}$$

$$\mathbf{D}(\mathbf{r},t) = \frac{1}{2}\mathbf{D_0}\exp(i(\mathbf{kr}-\omega t)) + \text{c.c.}, \tag{2.9}$$

$$\mathbf{B}(\mathbf{r},t) = \frac{1}{2}\mathbf{B_0}\exp(i(\mathbf{kr}-\omega t)) + \text{c.c.}, \tag{2.10}$$

where $\mathbf{E_0}$, $\mathbf{H_0}$, $\mathbf{D_0}$ and $\mathbf{B_0}$ are complex amplitudes, 'c.c.' denotes complex conjugate, and the following constitutive relations hold:

$$\mathbf{D_0} = \epsilon(\omega)\mathbf{E_0}, \tag{2.11}$$

$$\mathbf{B_0} = \mu(\omega)\mathbf{H_0}. \tag{2.12}$$

Substituting eqs. (2.7)–(2.12) into Maxwell's equations[3], we obtain:

$$\mathbf{k}\times\mathbf{E} = \mu(\omega)\frac{\omega}{c}\mathbf{H}, \tag{2.13}$$

$$\mathbf{k}\times\mathbf{H} = -\epsilon(\omega)\frac{\omega}{c}\mathbf{E}. \tag{2.14}$$

The system of eqs. (2.13) and (2.14) has a nontrivial solution if and only if the following condition holds:

$$k^2 \equiv (\mathbf{k}\cdot\mathbf{k}) = \epsilon(\omega)\mu(\omega)\frac{\omega^2}{c^2}, \tag{2.15}$$

which is the dispersion equation for electromagnetic waves the medium.

[3]In this work, we use Gaussian units, unless specified otherwise.

For simplicity, let us assume that there is no absorption (or it can be neglected), meaning that $\epsilon(\omega)$ and $\mu(\omega)$ are real ($\epsilon = \epsilon^*,\ \mu = \mu^*$). For wave propagation to be possible, the wavenumber k must be real ($k^2 > 0$), which, according to the dispersion equation (2.15), implies that ϵ and μ are either both positive or both negative. We shall consider these two possibilities.

From eqs. (2.13) and (2.14) it follows that the vectors $\mathbf{E}, \mathbf{H}, \mathbf{k}$ form a right-handed triplet (meaning that $\mathbf{k} \cdot (\mathbf{E} \times \mathbf{H}) > 0$[4]) for conventional materials with $\epsilon > 0,\ \mu > 0$ and a left-handed triplet ($\mathbf{k} \cdot (\mathbf{E} \times \mathbf{H}) < 0$) for double-negative materials. All media supporting propagating waves can thus be classified as right-handed (most of natural materials) and left-handed (negative-index materials being the prime example)[5]. The phase velocity $\mathbf{v}_{\mathrm{ph}}$ has the same direction as the wavevector $\mathbf{k}$ (by definition, $v_{\mathrm{ph}}^{(\alpha)} = \omega/k^{(\alpha)},\ \alpha = x, y, z$). On the other hand, the energy flow is determined by the Poynting vector [8]:

$$\mathbf{S} = \frac{c}{4\pi} \mathbf{E} \times \mathbf{H}, \tag{2.16}$$

which always forms a right-handed triplet with $\mathbf{E}$ and $\mathbf{H}$. Therefore, the direction of the energy flow coincides with the phase velocity for right-handed materials and is opposite to it in left-handed materials.

It would seem that simultaneously negative ϵ and μ imply negative electromagnetic energy density

$$W = \frac{1}{8\pi} \left(\epsilon \mathbf{E}^2 + \mu \mathbf{H}^2 \right), \tag{2.17}$$

which violates a fundamental requirement for it to be positive-definite, and thus such materials cannot exist. However, it actually means only that they must necessarily be dispersive, since formula (2.17) was derived derived for non-dispersive media. If one considers dispersive media instead, when the group velocity is well-defined and absorption can be neglected, then the expression for time-averaged energy density in quasimonochromatic waves becomes as follows [8]:

$$\overline{W} = \frac{1}{16\pi} \left(\frac{\partial(\epsilon\omega)}{\partial\omega} \left|\mathbf{E_0}\right|^2 + \frac{\partial(\mu\omega)}{\partial\omega} \left|\mathbf{H_0}\right|^2 \right), \tag{2.18}$$

where $\mathbf{E_0}$ and $\mathbf{H_0}$ are the complex amplitudes (see eqs. (2.7) and (2.8)) at the carrier frequency ω_0 and the derivatives are taken at the same point. From eq. (2.18), one can derive the necessary condition for the quadratic form of energy to be positive-definite:

$$\frac{\partial(\epsilon\omega)}{\partial\omega}|_{\omega_0} > 0,\ \frac{\partial(\mu\omega)}{\partial\omega}|_{\omega_0} > 0. \tag{2.19}$$

Equation (2.19) implies that materials with negative $\epsilon(\omega)$ and $\mu(\omega)$ must have sufficiently strong normal dispersion of those parameters, i.e. $\partial\epsilon/\partial\omega > 0$ and $\partial\mu/\partial\omega > 0$ [8].

[4] With this condition, one can generalise the concept of right-handed and left-handed materials to anisotropic media, where $\mathbf{S}$ and $\mathbf{k}$ are generally not collinear.

[5] The term 'left-handed materials' can be sometimes used in a broader sense for more general structures, e.g. photonic crystals [6] or anisotropic waveguides [7], with negative phase velocity in the energy flow direction. This discussion is outside the scope of this work, though.

The energy flow, as we have discussed, is related to the group velocity. Let us calculate the latter and investigate how the directions of the phase and group velocity are related. Without loss of generality, let us assume that a plane monochromatic wave propagates in the positive direction of the wavevector $\mathbf{k}$. The wavenumber k in this case, according to eq. (2.15), is given by:

$$k = \sqrt{\epsilon(\omega)\mu(\omega)}\frac{\omega}{c}. \tag{2.20}$$

The group velocity is defined as $\mathbf{v}_\mathrm{g} = \partial\omega/\partial\mathbf{k}$, so its component along the vector $\mathbf{k}$ is:

$$v_\mathrm{g} = \frac{\partial\omega}{\partial k} = 2c\sqrt{\epsilon\mu}\left(\mu\frac{\partial(\epsilon\omega)}{\partial\omega} + \epsilon\frac{\partial(\mu\omega)}{\partial\omega}\right)^{-1}. \tag{2.21}$$

First of all, it follows from eq. (2.21) that the group velocity can only be antiparallel to the phase velocity if frequency dispersion is present — indeed, without dispersion the phase and group velocities are equal. Moreover, the condition for v_g to be negative is automatically fulfilled for negative $\epsilon(\omega)$ and $\mu(\omega)$ due to eq. (2.19), and we can see that the particular case of electromagnetic waves is consistent with the general reasoning about phase and group (or energy) velocities.

When considering refraction, it is important to account for the type of materials involved, i.e. if they are right-handed or left-handed. Historically, Snell's law (2.6) was formulated for conventional materials in the form

$$n\sin\varphi = n_1\sin\varphi_1, \tag{2.22}$$

where the refractive index n is defined as $n = c/v_\mathrm{ph} = \sqrt{\epsilon\mu}$, according to eq. (2.15) (moreover, for optical frequencies usually $\mu(\omega) = 1$ in natural substances). In order to generalise Snell's law (2.6) for both right-handed and left-handed materials, the traditional definition of the refractive index should be altered the following way:

$$n = p\sqrt{\epsilon\mu}, \tag{2.23}$$

where $p = 1$ for right-handed materials ($\epsilon > 0,\ \mu > 0$) and $p = -1$ for left-handed materials ($\epsilon < 0,\ \mu < 0$). Since the refractive index n is negative for $\epsilon < 0,\ \mu < 0$, such materials are also referred to as negative-index materials.

For example, one can observe from eq. (2.22) that the refraction from vacuum ($n = 1$) to a negative-index medium occurs at a negative angle (fig. 2.1), while in a general case of two materials the phenomenon depends on p for each medium.

It is not only refraction that is different from conventional media in negative-index materials. Other optical phenomena change as well: for example, the Doppler and Cherenkov effects are inverted [2].

2.2 Experimental implementation of a negative-index metamaterial

In his work [2], Veselago not only considered the properties of negative-index materials, but also put forth suggestions as to where to search for them. Nevertheless, those predictions

were not fulfilled, and the subject had been mostly forgotten until an experimental demonstration of a new type of medium — a composite metamaterial containing wires and split-ring resonators which displayed simultaneously negative ϵ and μ in a certain microwave frequency range [9] (fig. 2.3). Negative refraction has also been demonstrated experimentally [10].

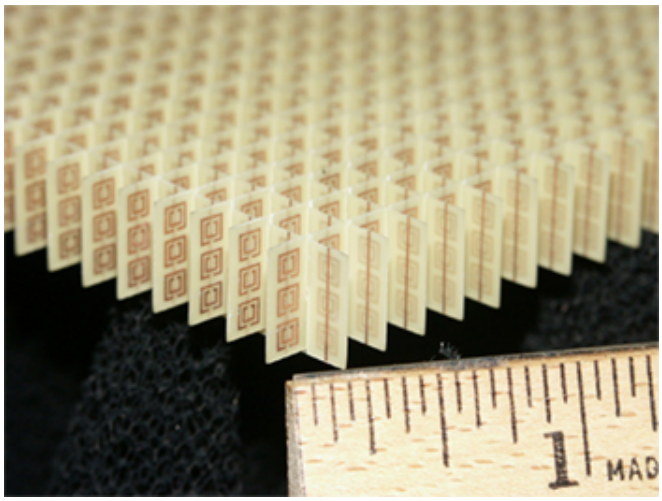

Figure 2.3: *One of the first negative-index materials consisting of wires and split-ring resonators [9]*

We shall focus on the building blocks of the metamaterial in question [9] to illustrate the main design philosophy of metamaterials — engineering desired properties based on the elementary units, or meta-atoms.

2.2.1 Wire medium for negative dielectric permittivity

An artificial medium composed of long parallel wires has been known for a long time [11]. After the construction of the first double-negative metamaterial [9], a generic plasma-type frequency dependence was used in a follow-up paper [12] to describe the effective permittivity:

$$\epsilon_{\text{eff}} = 1 - \frac{\omega_{\text{p}}^2}{\omega^2}, \tag{2.24}$$

where ω_{p} is dependent on the geometry of wires.

A more thorough theoretical description, however, was provided later [13]. The authors derive from first principles an exact expression for ϵ_{eff} in a quasi-static model. From circuit theory, once can obtain:

$$\mathbf{D} = \left(\bar{\bar{I}} - \frac{4\pi c^2 \mathbf{e}_z \mathbf{e}_z}{\omega^2 a^2 L} \right) \mathbf{E} = \bar{\bar{\epsilon}}_{\text{eff}} \mathbf{E}, \tag{2.25}$$

where the wires of radius r_0 are positioned along the unit vector $\mathbf{e}_z$ at the distance a between each other and L is the wire inductance per unit length:

$$L = 2 \ln \frac{a^2}{4r_0(a - r_0)}. \tag{2.26}$$

When the wires are in an effective magnetic medium described by the magnetic permeability $\mu(\omega)$, the inductance (2.26) is multiplied by μ. If the magnetic permeability is negative, then the condition for a negative refractive index cannot be achieved, since the dielectric permittivity in eq. (2.25) become positive-definite instead of the plasma-like frequency dependence (2.24). This leads to a question: is it at all possible to use the wire medium for constructing a double-negative metamaterial?

So far we have assumed that the magnetic medium is continuous. However, the implementation of a material with negative μ consists of magnetic meta-atoms, such as split-ring resonators discussed below in section 2.2.2. The effective magnetic permeability is then obtained by simple homogenisation. Generally, this is a valid assumption, since the meta-atoms are of subwavelength size. For the negative-index metamaterial in question, however, the microscopic structure is important. If the split-ring resonators are placed symmetrically between the wires, where the magnetic field from the currents in the wires is zero, then the effect of the resonators on the permittivity is very small. Nevertheless, it is insightful that the properties of a metamaterial are not always defined simply by the averaged properties of meta-atoms: the interaction between structural elements, which are designed separately for their own purposes, can be important and yield new effects of their own interest. We shall discuss another example of this kind in section 2.3.

2.2.2 Split-ring resonators for negative magnetic permeability

Proposed by Pendry *et al* [14], a split-ring resonator (SRR) is probably the most recognised and archetypical 'meta-atom' element. It is also an excellent demonstration of how the ideas of classical electrical engineering, such as circuit theory, helped form the staple in the framework of metamaterial design.

The basic physics governing the operation principles of a SRR can be expressed in a very simple way. The resonator itself acts like an LC-circuit, with the inductance arising from the geometry of the rings and the capacitance being created mainly by the gaps (fig. 2.4). The resonant frequency is thus defined by geometrical features. The magnetic field perpendicular to the plane of the resonator creates, according to Lenz's law, a current in the rings, so that the SRR is a driven LC-circuit. Above the resonance, the magnetic response of the SRR is negative with respect to the driving force and large enough in magnitude so that the overall μ_{eff} (obtained by simple homogenisation) is negative.

The resulting expression for the magnetic permeability of a structure presented at fig. 2.3 (the SRRs in an elementary cell are arranged in two orthogonal arrays of planes which are parallel to the wires) is as follows [9, 14]:

$$\overline{\overline{\mu}}_{\text{eff}} = \overline{\overline{I}} - \frac{F\omega^2(\mathbf{e}_x\mathbf{e}_x + \mathbf{e}_y\mathbf{e}_y)}{\omega^2 - \omega_0^2 + i\omega\Gamma}, \tag{2.27}$$

where ω_0 is the resonance frequency, Γ corresponds with losses and F is a parameter dependent on the geometry of the rings.

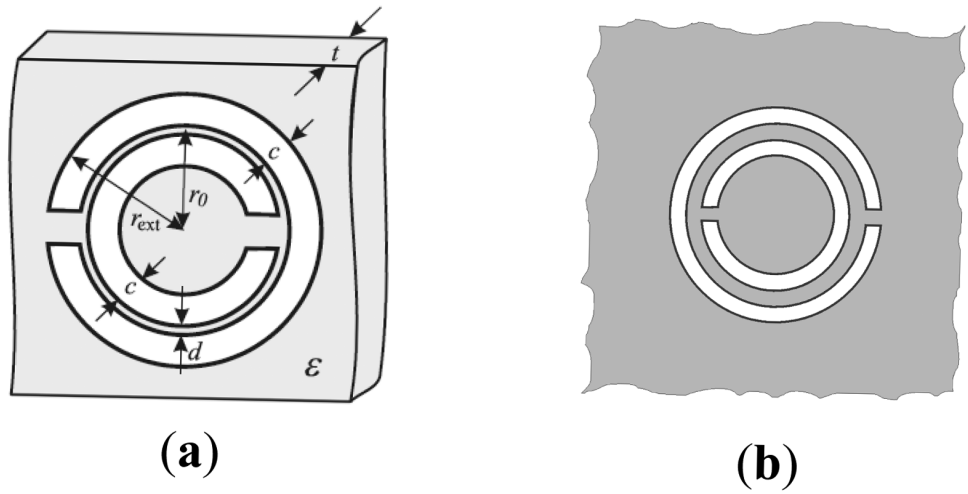

Figure 2.4: *Example geometries of typical metallic (a) and so-called complementary (b) split-ring resonators from the review by Martín and Bonache [15]. Characteristic parameters of the structure are shown on the figure.*

2.3 Metamaterial developments beyond negative refraction

Since the pioneering experiments mentioned above [9, 10], the emerging field of metamaterials has undergone explosive growth. Reviewing the progress made in the confines of this thesis is akin to skimming the surface of the vast sea of knowledge. Nevertheless, we shall overview some of the important directions and developments in this area.

Going from microwave to optical range has proved challenging. Many of the traditional approaches, like those discussed above, are no longer valid, since metals can no longer be considered as perfect or almost perfect conductors. Electromagnetic field penetrates into the metal due to the skin effect, and at high frequencies the penetration depth becomes comparable with the size of the elements. As a result, geometry is no longer defining the properties. It is also much harder to implement subwavelength meta-atoms for optical frequencies, since it requires advanced nanofabrication techniques.

Nevertheless, it has been possible to move from microwave to terahertz and even optical regime. Shalaev reviews the progress in optical negative-index materials (NIMs) [16], while also discussing such issues as tunability, gain (particularly important for plasmonic NIMs due to high losses) and nonlinear phenomena. Soukoulis and Wegener in their survey [17] contemplate such problems as constructing optical metamaterials — both plasmonic and dielectric, i.e. free of metallic components and their inherent loss issues. Another problems discussed in their review are building fully-fledged 3D metamaterials and active loss compensation (with gain media). They consider also fabrication techniques and applications, such as superlensing (the idea of a superlens — i.e. a lens capable of

focusing beyond the diffraction limit — based on negative-refraction metamaterials was proposed by Pendry [18]).

Lapine and Tretyakov in their notes [1] discuss both conceptual issues of metamaterials, such as definition, basic theory, generic chiral metamaterials, etc, and applied problems, such as transmission-line realisations of metamaterials and applications for superlensing, among others. Engheta, Ziolkowski *et al* explore the progress in various fields of metamaterial development with close attention to engineering aspects [19], e.g. antennae or waveguide applications, among others.

As for engineering, so far we have observed the strong influence of electrical engineering concepts, such as circuits or transmission lines (in case of e.g. long wires), on metamaterials design. However, attempts have been made to do the opposite, i.e. implement the systems already known in conventional circuit theory, but with optical elements. Engheta reviews the progress made on this path [20] in a developing field dubbed metatronics [21].

Moreover, backward waves in NIMs, meaning anti-parallel phase and group velocity, have inspired the development of so-called left-handed transmission lines (reviewed also by Engheta, Ziolkowski *et al* [19]), the dispersion properties of which strongly resemble those of double-negative media. This is another example how very fundamental concepts, i.e. left-handed media described by Veselago [2], can be sometimes transferred to applied fields and provide new insights — with successful implementations — to such well-known and staple concepts of electrical engineering as transmission lines.

Previously we have mentioned how the interaction between meta-atoms can result in cardinally different phenomena than one would expect from simple homogenisation based on individual meta-atom properties. A prime example is magnetoinductive waves: under certain circumstances, an array of split-ring resonators might not behave at all as predicted by the theory for μ_{eff} outlined above. Upon detailed scrutiny, it turns out that the magnetic coupling between adjacent elements in such arrays plays a key role, giving rise to a new type of phenomena — so-called magnetoinductive waves. While these phenomena completely ruin the predictions of the effective-medium theory, they could instead be harnessed and exploited; an article by Shamonina and Solymar [22] reviews the progress and applications of those magnetoinductive waves.

So far we have considered (or silently assumed) mostly bulky, three-dimensional metamaterials. However, due to such issues as losses or fabrication challenges, flat two-dimensional structures are sometimes more desirable. Such 2D metamaterials are known as metasurfaces (various structures of this kind are reviewed in a book by Engheta, Ziolkowski *et al* [19]). Moreover, the area of so-called flat optics has been developed [23], making use of them instead of traditional lenses and other bulky systems. Some other approaches to 2D optics include surface waves on metasurfaces [24], the impedance of the latter being controlled e.g. by the printing process. It has also been demonstrated that, under certain circumstances, graphene can act as a metasurface [25, 26] for such applications as transformation and flat Fourier optics.

This is but a brief review of some important directions and developments in the field of metamaterials. Nevertheless, it is clear that the common theme is designing artificial structural elements for any particular purpose — the range of the latter has expanded far beyond the original interest in negative-index materials, for example.

2.4 Tunable metamaterials for potential implementations of time-dependent media

Previously the importance of tunability for metamaterials [16] was mentioned very briefly. Let us elaborate on the matter in detail.

A split-ring resonator considered in section 2.2.2, for example, has a fixed resonance frequency defined by the geometry. It implies that a medium composed of SRRs exhibits the desired property — namely negative effective magnetic permeability — only in a rather narrow frequency range. However, for potential applications this constitutes a major drawback, and tunability in general — i.e. the ability to change the properties of metamaterials 'on the fly' — is much sought after in metamaterial design.

Moreover, for implementing the phenomena discussed in Paper 1, there is an additional requirement. Not only must the properties (such as ϵ and μ) of a metamaterial be variable with time, but they are also to be changed *fast enough*, so that the system cannot be treated as quasi-static with respect to ϵ and μ, and the effects discussed are significant. While extensive reviews of tunable metamaterials in general [27, 28] and michromachined tunable metamaterials in particular, as well as their fabrication techniques [29], are available, let us discuss the open issue of tunable metamaterials suited for potential implementations of time-dependent media.

A simple approach is mechanical reconfiguration, i.e. changing the positions of the elements, for example by electrical or other forces, such as optical. Although this approach might be useful for tunable metamaterials (typically in the GHz and THz ranges) in general, it seems problematic for the task at hand: a typical response time of micromachined metamaterials in the THz range is sub-milliseconds [29], meaning that they are not suitable for applications where fast modulation is of the essence, as is the case in this work. Slower effects (e.g. thermal) are out of the question for the same reason.

A somewhat more promising approach based on changing metamaterial properties via photoconductivity has been proposed for terahertz metamaterials [30, 31]. While the structures in question could be useful on their own for bridging the so-called terahertz gap, they are of interest to us because they are completely optically switchable (tunable). The effectiveness of such metamaterials for implementing time-dependent systems remains to be investigated.

As with other metamaterial applications, considering metasurfaces instead of bulky materials can be advantageous. A tunable teraherts meta-surface with graphene cut-wires has been proposed [32]; moreover, tunable terahertz frequency comb generation using time-dependent graphene sheets has been demonstrated numerically [33].

As for optical frequencies, we a treading into an unknown field. However, numerical modelling of devices with the method decribed in Chapter 3 can help determine necessary constraints and limitations for potential design and fabrication of appropriate metamaterials.

3 Modelling time-dependent metamaterials with the Finite-Difference Time-Domain method

Since our analytical knowledge of time-varying media is limited, studying their properties numerically is an obvious choice. This is especially true in the light of computing power available nowadays, as opposed to the era when the Finite-Difference Time-Domain (FDTD) method was first developed [34].

For simplicity's sake, let us consider an isotropic, non-dispersive, linear medium. In this case, its electromagnetic properties can be described in terms of two scalar functions — dielectric permittivity ϵ and magnetic permeability μ, which are, generally speaking, functions of time. This implies that Maxwell's equations should be solved in the time domain, since frequency-domain methods, *despite linearity*, are not applicable. On the contrary, with the time-domain approach, as will be demonstrated in the following, the temporal dependence of ϵ and μ can be handled in a natural way.

With the choice of method having been made, it is possible to focus on the numerical implementation and applications.

In this chapter, the general ideas of the FDTD method are outlined first. After that we focus on some important aspects of numerical modelling, namely source and boundary conditions, as well as the practical implementation.

3.1 From Maxwell's equations to the FDTD method

3.1.1 Theoretical introduction; the role of dispersion and inhomogeneity in space and time

In their most general differential form, Maxwell's equations are written as:

$$\nabla \times \mathbf{H} = \frac{1}{c}\frac{\partial \mathbf{D}}{\partial t} + \frac{4\pi}{c}\mathbf{j}, \tag{3.1}$$

$$\nabla \times \mathbf{E} = -\frac{1}{c}\frac{\partial \mathbf{B}}{\partial t}, \tag{3.2}$$

$$\nabla \cdot \mathbf{D} = 4\pi\rho, \tag{3.3}$$

$$\nabla \cdot \mathbf{B} = 0. \tag{3.4}$$

In eqs. (3.1)–(3.4), $\mathbf{E}$ and $\mathbf{B}$ are the averaged microscopic electric and magnetic fields respectively, and $\mathbf{D}$ and $\mathbf{H}$ are defined the following way:

$$\mathbf{D} = \mathbf{E} + 4\pi\mathbf{P}, \tag{3.5}$$

$$\mathbf{H} = \mathbf{B} - 4\pi\mathbf{M}, \tag{3.6}$$

where the polarisation $\mathbf{P}$ and magnetisation $\mathbf{M}$ correspond with the average electric and magnetic dipole moments of bound charges and currents per unit volume in medium. The

averaging is understood in the following way: in order to obtain the macroscopic fields, the microscopic quantities are averaged over some characteristic distance l, which is much bigger than the characteristic atomic (or equivalent) size a, but much smaller than the characteristic wavelength λ of the electric field:

$$a \ll l \ll \lambda. \tag{3.7}$$

It means that instead of a microscopic model consisting of atoms or other elements, an effective homogeneous — at the scale of l — medium is considered. A similar averaging procedure is also performed in time with the following hierarchy of scales:

$$t_a \ll \tau \ll T, \tag{3.8}$$

where t_a is the characteristic atomic response time, T is the characteristic period and the averaging (homogenisation) is done on the scale of τ.

Combined with the constitutive relations between $\{\mathbf{D}, \mathbf{B}\}$ and $\{\mathbf{E}, \mathbf{H}\}$, initial and boundary conditions, eqs. (3.1)–(3.4) provide a unique and complete solution for the electromagnetic problem.

Note: Sometimes a symmetric 'magnetic current' term is introduced to the right-hand side of eq. (3.2), as well as the respective magnetic conductivity in the 'magnetic Ohm's law'. This, however, is only a mathematical model, since no magnetic charges have been observed, and the real physical field $\mathbf{B}$ is always divergence-free.

An example of a constitutive relation is a model of linear dielectric permittivity. In this case, the polarisation $\mathbf{P}$ is related only to the electric field[1] $\mathbf{E}$ in a linear fashion. The most general expression satisfying the causality condition has the following form:

$$\mathbf{P}(\mathbf{r}, t) = \int_V \int_0^{+\infty} \hat{\chi}(\mathbf{r}, \mathbf{r}'; t, t') \mathbf{E}(\mathbf{r} - \mathbf{r}', t - t') \mathbf{dr}' dt'. \tag{3.9}$$

One can observe that eq. (3.9) accounts for both temporal and spatial inhomogeneities and non-localities simultaneously. However, it is convenient to investigate particular cases first and thus get an understanding of the whole. Therefore, we shall consider the aforementioned effects separately side-by-side in order to demonstrate the analogy between the electromagnetic response in time and space and the role of time-dependent electromagnetic materials — a somewhat unconventional concept in traditional electrodynamics[2] — in the general theoretical picture.

Considering only the spatial dependence of the response, one can write in the most general form:

$$\mathbf{P}(\mathbf{r}) = \int_V \hat{\chi}(\mathbf{r}, \mathbf{r}') \mathbf{E}(\mathbf{r} - \mathbf{r}') \mathbf{dr}', \tag{3.10}$$

where the convolution kernel $\hat{\chi}$ is a tensor, and the integration is performed over the whole physical volume, i.e. formally from $-\infty$ to $+\infty$ for each coordinate, although $\hat{\chi}$

[1] Generally speaking, this is not always the case for metamaterials. For so-called chiral or generic bi-isotropic/bi-anisotropic media, the electric and magnetic responses might be coupled [35, 36]. We do not discuss such media here, though.

[2] Paper 1 provides a literature review of systems where explicit time dependence of electromagnetic properties is of importance.

decreases with $\mathbf{r}'$, meaning that the integral is taken effectively over a finite area of non-local response.

The non-local response in eq. (3.10) results in spatial dispersion, which is a defining characteristic of some systems, such as plasma in magnetic field, gyrotropic (optically active) media and even graphene, among others. However, for many substances such as common dielectrics, spatial dispersion is negligible. The main physical reason for it is that the non-local response effectively vanishes even at distances comparable to l, meaning that the macroscopic description is essentially local *by definition*. In this case,

$$\hat{\chi}(\mathbf{r}, \mathbf{r}') = \hat{\chi}(\mathbf{r})\delta(\mathbf{r}'), \tag{3.11}$$

and we have a simple relation:

$$\mathbf{D}(\mathbf{r}) = (1 + 4\pi\hat{\chi}(\mathbf{r}))\mathbf{E}(\mathbf{r}) = \hat{\epsilon}(\mathbf{r})\mathbf{E}(\mathbf{r}). \tag{3.12}$$

Let us consider the other particular case instead — that of a strongly non-local response, however, with the kernel of the polarisation operator in eq. (3.10) having translational symmetry, i.e. being independent of $\mathbf{r}$. In this case, due to the Fourier property of the convolution integral, one can write in the Fourier space:

$$\mathbf{P}(\mathbf{k}) = \hat{\chi}(\mathbf{k})\mathbf{E}(\mathbf{k}) \tag{3.13}$$

and

$$\mathbf{D}(\mathbf{k}) = (1 + 4\pi\hat{\chi}(\mathbf{k}))\mathbf{E}(\mathbf{k}) = \hat{\epsilon}(\mathbf{k})\mathbf{E}(\mathbf{k}). \tag{3.14}$$

Generally, even for isotropic media the tensor nature of $\hat{\epsilon}(\mathbf{k})$ is important, since the wavevector $\mathbf{k}$ itself creates a distinct direction in space.

It is interesting to compare homogeneous media with spatial dispersion with some local, yet inhomogeneous structures. For example, in so-called photonic crystals the macroscopic dielectric permittivity $\epsilon(\mathbf{r})$, which is usually local, varies periodically on the scale of the wavelength. The dispersion of a photonic crystal as a whole $\omega = \omega(\mathbf{k})$ is strongly dependent on the wavevector $\mathbf{k}$. In some cases, even an effective permittivity $\epsilon_{\text{eff}}(\mathbf{k})$ can be introduced to describe the behaviour of light in a photonic crystal, as though it were a continuous medium. However, the nature of the effect is completely different from the nonlocalal response of spatially dispersive constituent materials. Another example is a simple waveguide made of an isotropic local dielectric, such as fused quartz. It is not the material, but the geometry that results in a single preferred propagation direction.

If only the temporal dependence is considered instead, then one obtains:

$$\mathbf{P}(t) = \int_0^{+\infty} \hat{\chi}(t, t')\mathbf{E}(t - t')dt'. \tag{3.15}$$

Notice the difference between eq. (3.10) and eq. (3.15): due to causality considerations, the integration is done only for the positive half-line of delay times t', however, the rest of the properties are analogous to the space domain.

Without loss of generality, one can re-write eq. (3.15) the following way:

$$\mathbf{P}(t) = \int_0^{+\infty} \hat{\chi}(t,t') \int d\omega \mathbf{E}(\omega) \exp(-i\omega(t-t'))dt', \tag{3.16}$$

where the integration is performed over all frequencies. Let us also assume the absolute convergence of the integrals, which is generally the case for physically reasonable models, e.g. a Gaussian field spectrum $\mathbf{E}(\omega)$ and exponentially decaying $\hat{\chi}(t,t')$ at $t' > \tau_0$, where τ_0 is the characteristic 'memory time' of the medium. The integration order in eq. (3.16) can then be changed, and we obtain:

$$\mathbf{P}(t) = \int d\omega \mathbf{E}(\omega)\hat{\chi}(t,\omega) \exp(-i\omega t), \tag{3.17}$$

where

$$\hat{\chi}(t,\omega) \equiv \int_0^{+\infty} dt' \hat{\chi}(t,t') \exp(i\omega t'). \tag{3.18}$$

For conventional dispersive, time-invariant media (meaning that $\hat{\chi}(t,\omega)$ does not depend on t) eq. (3.17) is reduced to the familiar expression, analogous to eq. (3.13):

$$\mathbf{P}(\omega) = \hat{\chi}(\omega)\mathbf{E}(\omega), \tag{3.19}$$

and

$$\mathbf{D}(\omega) = (1 + 4\pi\hat{\chi}(\omega))\mathbf{E}(\omega) = \hat{\epsilon}(\omega)\mathbf{E}(\omega). \tag{3.20}$$

Temporal, or frequency, dispersion is often more pronounced and important than spatial dispersion for common substances used in optics. The fact that the electric response is not local in time, i.e not instantaneous, results in polarisation's being proportional to the electric field in frequency domain, but not in time domain in general. If time translation symmetry, or invariance, is also broken, then only expression (3.17) is generally valid. Let us investigate the conditions under which the polarisation is nevertheless proportional to the electric field in time domain. For clarity, let us also assume that $\hat{\chi}(t,\omega)$ is a real function[3].

For many important applications, the spectrum of electromagnetic radiation is finite with the spectral width $\delta\omega$ and centered around some characteristic carrier frequency ω_0 on the positive half of the spectrum (due to Fourier properties of a real function, the negative half is symmetric). Nanosecond and even picosecond laser pulses are a good example, which is also of practical interest for telecommunication systems and other applications. If the dielectric susceptibility has a 'plateau' in the frequency range in question, i.e.

$$\left| \frac{\hat{\chi}(t,\omega) - \hat{\chi}(t,\omega_0)}{\hat{\chi}(t,\omega_0)} \right| \ll 1 \tag{3.21}$$

[3]This is the case when losses can be neglected, however, it is not a *necessary* condition, since absorption can be described by either complex dielectric permittivity or electric conductivity. In the second formalism, the expression for losses essentially coincides with Ohm's law, however, it does not imply a physical current of free charges: thus introduced electric conductivity can be considered just as a formal way to define absorption. Analogously, the magnetic losses can be described in terms of either complex magnetic permeability or magnetic conductivity, thus the 'magnetic current', even that no physical magnetic charges have been observed so far. The choice of either formalism depends on the application. We shall return to this question when we discuss the FDTD method in particular.

for $|\omega - \omega_0| \leqslant \delta\omega$, then it is possible to approximate eq. (3.17) the following way:

$$\mathbf{P}(t) = \hat{\chi}(t, \omega_0)\mathbf{E}(t) = \hat{\chi}(t)\mathbf{E}(t), \tag{3.22}$$

and

$$\mathbf{D}(t) = (1 + 4\pi\hat{\chi}(t))\mathbf{E}(t) = \hat{\epsilon}(t)\mathbf{E}(t). \tag{3.23}$$

One can also observe that the expression (3.22) is *exact* for monochromatic waves. If the field $\mathbf{E}(t) = \mathbf{E_0}(t)\exp(-i\omega_0 t) + \text{c.c.}$ is quasimonochromatic and the envelope $\mathbf{E_0}(t)$ is varying slowly on the scale of τ_0, then we also obtain the same result (3.22), although the restrictions on the spectral width $\delta\omega$ in this case can be stronger than in eq. (3.21). Finally, if $\hat{\chi}(t, t')$ decays as a function of t' much faster than the characteristic variation of the field, i.e. $\omega_0\tau_0 \ll 1$, then it acts like a delta-function in eq. (3.18), meaning that the response is almost instantaneous, and we obtain:

$$\mathbf{P}(t) = \hat{\chi}(t, 0)\mathbf{E}(t) = \hat{\chi}(t)\mathbf{E}(t). \tag{3.24}$$

This result means that the model of a local temporal response, analogous to eqs. (3.11) and (3.12), physically corresponds with the low-frequency (or essentially static) limit of the dispersive electric susceptibility (3.18).

Although the expressions (3.22) and (3.24) have the same form, there is an important difference: although explicit frequency dispersion is neglected in the former, non-locality is still accounted for in it by estimating the susceptibility $\hat{\chi}(t, \omega)$ at the frequency ω_0 and *not* at zero frequency, while the latter is strictly local. In the following we shall understand dispersionless media in the former, broader sense when it comes to the response in time.

By combining the results for media without spatial and temporal dispersion, as discussed above, and assuming also an isotropic case (meaning that χ is scalar), we obtain a simple constitutive relation to base our numerical scheme on:

$$\mathbf{D}(\mathbf{r}, t) = (1 + 4\pi\chi(\mathbf{r}, t))\mathbf{E}(\mathbf{r}, t) = \epsilon(\mathbf{r}, t)\mathbf{E}(\mathbf{r}, t). \tag{3.25}$$

The magnetic response, described by the magnetic permeability μ, can be considered analogously:

$$\mathbf{B}(\mathbf{r}, t) = (1 + 4\pi\chi_m(\mathbf{r}, t))\mathbf{H}(\mathbf{r}, t) = \mu(\mathbf{r}, t)\mathbf{H}(\mathbf{r}, t). \tag{3.26}$$

The model is consistent if $\epsilon(t)$ and $\mu(t)$ are varying slowly, so that all the fields remain in the operating frequency range $|\omega - \omega_0| \leqslant \delta\omega$.

3.1.2 Discrete equations for the numerical scheme

In order to grasp the main ideas of the numerical method, let us start with the most simple case of a linear, lossless, non-dispersive, isotropic medium, which can be described in terms of two parameters: dielectric permittivity ϵ and magnetic permeability μ. We note that in time domain these material parameters are real functions, and losses are described e.g. in terms of conductivity rather than complex dielectric permittivity. The plethora of other phenomena hidden in the constitutive relations behind the apparent simplicity of eqs. (3.1)–(3.4) can be considered afterwards, once the basic technique has been developed. Moreover, we can start with the two-dimensional case (translational

symmetry along the z direction). It is well-known [37] that in this case the field equations split into two independent sets, corresponding with TM_z (which consists of H_x, H_y and E_z field components) and TE_z (E_x, E_y and H_z) modes respectively.

For numerical purposes it is more convenient to utilise dimensionless units. In this particular case, we choose them in such a way that that $c = 1$: firstly, this eliminates redundant constants such as c (or ϵ_0, μ_0, etc if using SI units); secondly, operating with relative units such as 'cells per wavelength' is more natural from the computational point of view and has the added benefit of accounting for similarity criteria in physical systems.

Under the assumptions made above, Maxwell's equations for the TM_z mode take the form:

$$\frac{\partial}{\partial t}\left(\mu H_x\right) = -\frac{\partial E_z}{\partial y}, \tag{3.27}$$

$$\frac{\partial}{\partial t}\left(\mu H_y\right) = \frac{\partial E_z}{\partial x}, \tag{3.28}$$

$$\frac{\partial}{\partial t}\left(\epsilon E_z\right) = \frac{\partial H_y}{\partial x} - \frac{\partial H_x}{\partial y}. \tag{3.29}$$

The other mode, TE_z, can be considered analogously.

We must note that for materials that are both time-dependent and dispersive in time, due to the nature of the numerical method chosen, the convolutional expression (3.15) must be operated with directly instead of working in frequency domain. For a numerical scheme to be efficient, the convolution integrals must be evaluated in an appropriate way, rather than computing them directly. The methods to do so are well-known for some common dispersion models, such as Drude, Lorentz and Debye media [37]. However, this issue lies outside the current scope of this work.

Before we focus on the details of a concrete numerical scheme, let us discuss a fundamental invariant following from Maxwell's equations, which must also pertain to physically reasonable numerical methods. An important particular case is the absence of free charges and currents, which corresponds to e.g. propagation of optical waves. In this case, the system's dynamics is determined only by eqs. (3.1) and (3.2), while the divergences of $\mathbf{D}$ and $\mathbf{B}$ are automatically zero at any time (one can immediately prove it by applying the divergence operator to eqs. (3.1) and (3.2)). This has an important practical implication: any discrete numerical scheme based on solving the curl equations, such as the classical Yee's scheme [34], should be intrinsically divergence-free. This holds true for Yee's original algorithm [37]; our generalisation of it for time-dependent metamaterials discussed below also satisfies this condition, which can be proved analogously.

In order to obtain discretised field update equations, we use the ideas of Kane Yee's original finite-difference time-domain (FDTD) method [34]. It is worth noting that, despite all the efforts and advances in numerical computational schemes throughout the decades, none of those contributions have had the longevity, impact and popularity of the pioneering one. Some of the reasons for it are that Yee's method is simple, robust, compatible with many other tools, such as advanced boundary conditions; another advantage is that the scheme in question has been studied thoroughly and practiced extensively, so that the amount of knowledge and experience available is vast.

The basic idea of Yee's method is to use central differences on a staggered grid (both in space and time, resulting in a leapfrog-like scheme), which is denoted traditionally by integer and half-integer indices (since the field values are staggered by a half step, such notation is also rather natural from a human viewpoint). The resulting cell in two and three dimension is presented graphically at fig. 3.1.

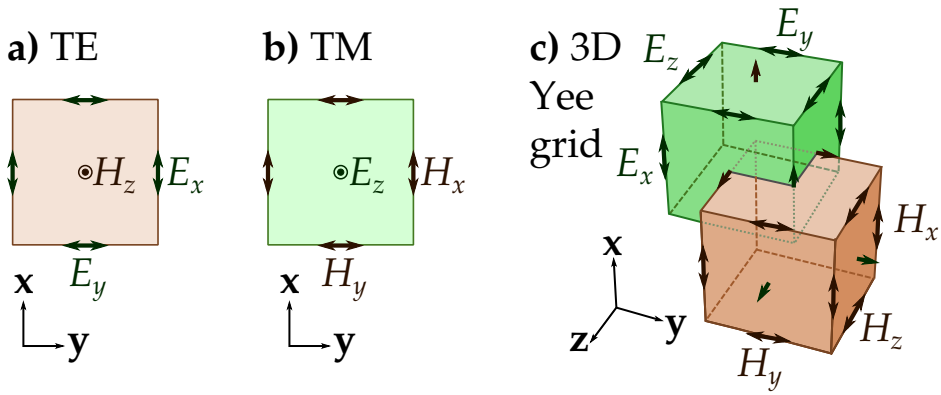

Figure 3.1: *A Yee cell in 2D and 3D (from Wikipedia)*

For our time-dependent eqs. (3.27)–(3.29), however, the values of fields and material parameters appear also outside their 'natural' time points in the additional terms arising from the temporal derivatives of ϵ and μ. In order to address the matter in a computationally effective way, we use the so-called semi-implicit approximation [37] (see also Paper 1 for a detailed explanation).

The resulting discretised update equations are as follows:

$$H_x|^{n+1/2}_{i,j+1/2} = \frac{1}{\mu|^{n+1/2}_{i,j+1/2}} \left[\mu|^{n-1/2}_{i,j+1/2} H_x|^{n-1/2}_{i,j+1/2} - \frac{\Delta t}{\Delta y} \left(E_z|^{n}_{i,j+1} - E_z|^{n}_{i,j} \right) \right], \tag{3.30}$$

$$H_y|^{n+1/2}_{i+1/2,j} = \frac{1}{\mu|^{n+1/2}_{i+1/2,j}} \left[\mu|^{n-1/2}_{i+1/2,j} H_y|^{n-1/2}_{i+1/2,j} + \frac{\Delta t}{\Delta x} \left(E_z|^{n}_{i+1,j} - E_z|^{n}_{i,j} \right) \right], \tag{3.31}$$

$$E_z|^{n+1}_{i,j} = \frac{1}{\epsilon|^{n+1}_{i,j}} \left[\epsilon|^{n}_{i,j} E_z|^{n}_{i,j} + \frac{\Delta t}{\Delta x} \left(H_y|^{n+1/2}_{i+1/2,j} - H_y|^{n+1/2}_{i-1/2,j} \right) - \right.$$
$$\left. - \frac{\Delta t}{\Delta y} \left(H_x|^{n+1/2}_{i,j+1/2} - H_x|^{n+1/2}_{i,j-1/2} \right) \right], \tag{3.32}$$

where $u|^{n}_{i,j} = u(i\Delta x, j\Delta y, n\Delta t)$ for any quantity u and i, j, n are integers.

From eqs. (3.30)–(3.32) it is obvious that only the dimensionless ratios $S_x = \Delta t/\Delta x$ and $S_y = \Delta t/\Delta y$ (they could be called 'partial Courant factors' for reasons discussed in the following) matter for the numerical scheme, which is also why the choice of dimensionless units discussed above is convenient.

The general Courant-Friedrichs-Lewy stability condition (the proof for the FDTD scheme, for example, can be found in the book by Taflove *et al* [37]) implies that

$$v^2(S_x^2 + S_y^2 + S_z^2) \leq 1, \tag{3.33}$$

where v is the speed of light in the material ($v = c = 1$ for free space; S_z is defined analogously for the 3D problem, in our case one can formally set it to zero; same holds true for a 1D reduction; the factor $S = \sqrt{S_x^2 + S_y^2 + S_z^2}$ is sometimes referred to as the Courant factor). Its applicability to the time-dependent scheme in question, as well as some general stability concerns, are discussed in detail in Paper 1.

3.2 Source and boundary conditions

It might appear from Section 3.1 that numerical modelling of various electromagnetic materials with the FDTD method is trivial, for Yee's scheme or variations thereof, such as eqs. (3.30)–(3.32), are rather simple and can be implemented with a few lines of code, eliminating the need for complex and often costly industrial software packages.

However, as a popular idiom has it, 'the devil is in the detail'. For example, the textbook on computational electrodynamics [37] — cited numerous times in this work — has several chapters, each of them dedicated to such 'trifling' matters and rivalling in volume the (very extensive) description of the method itself. When it comes to practical implementation, problems like an accurate description of various media types or geometry features can constitute the majority of the work being done and even be the main competitive features of commercial software.

In this section, we shall consider two basic numerical issues that arise when solving an electromagnetic scattering problem, namely getting the light into the computational domain and getting it out. These aspects are relevant to many practical applications in general and to our study of time-dependent media in particular. The solutions to those issues are the total-field / scattered-field sources and proper absorbing boundary conditions — perfectly matched layers — respectively, which we shall consider in the following.

3.2.1 Total-Field / Scattered-Field sources

In a scattering problem, one considers an incident wave which scatters at some object of interest. Introducing even the simplest type of such incident field — a plane monochromatic wave — into the computational domain is fraught with difficulties and challenges. Implementing a so-called 'hard' source, i.e. updating selected points of the grid according to the incident field, results in the source's being opaque for back-scattered waves. The 'hard' source itself acts like a mirror for the scattered field, generating spurious non-physical reflections. Inserting radiation as an initial condition might be feasible for confined pulses, but not for continuous waves, since it uses the crucial resource — computing memory — in the least efficient way.

A useful technique to solve this issue is to split the computational domain in two parts — one with total field $\vec{u}_t$, typically located in the middle of the grid, and another

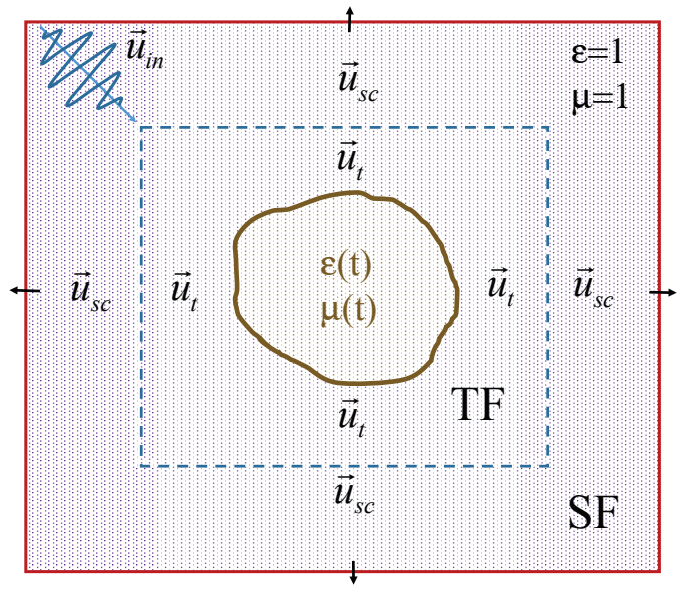

Figure 3.2: *The layout of the computational domain in the TF/SF technique. The scattering object (in the middle) is surrounded by vacuum (pink area). The whole domain is split into the TF and SF regions. The total $\vec{u}_t$ and scattered $\vec{u}_{sc}$ fields are present in their respective areas, and the incident field $\vec{u}_{in}$ is injected in the TF region. On the outer boundary, the scatter field is dealt with by the absorbing boundary conditions.*

where only the scattered field (SF) $\vec{u}_{sc}$, i.e. the difference between total field (TF) $\vec{u}_t$ and incident field $\vec{u}_{in}$, is present (see fig. 3.2); hence the name of the method — TF/SF. On the boundary between the two areas, the update equations (eqs. (3.30)–(3.32)) for the field must be corrected as described below, so that the boundary has the following properties: firstly, it acts like a Huygens surface, injecting the incident field into the TF subdomain; secondly, it is completely transparent to back-scattered radiation, which travels to the SF region and is usually absorbed by appropriate boundary conditions. This technique is well-known [37] and is suited for many applications, such as studying the field scattered by a particle or an antenna.

Let us consider the operating principle of TF/SF sources in detail. Due to linearity of eqs. (3.30)–(3.32), all the physical (total) fields can be represented as a sum of the incident field and the scattered field:

$$u_t = u_{in} + u_{sc}, \tag{3.34}$$

where $\vec{u} = \mathbf{E}, \mathbf{H}$, or, in case of the TM_z polarisation considered here, $u = E_z, H_x, H_y$, and

eqs. (3.30)–(3.32) can be solved separately for u_{in} and u_{sc} in the SF area.

However, on the very boundary between the total-field and the scattered-field area, an inconsistency arises. Let us assume that the left boundary of the TF area is located at the point i_l in vacuum, then eq. (3.31) reads:

$$H_y^{(sc)}|_{i_l-1/2,j}^{n+1/2} = H_y^{(sc)}|_{i_l-1/2,j}^{n-1/2} + \frac{\Delta t}{\Delta x}\left(E_z^{(t)}|_{i_l,j}^{n} - E_z^{(sc)}|_{i_l-1,j}^{n}\right). \tag{3.35}$$

In this expression, all but the third term, which is in the TF domain, belong to the SF domain (the upper index in brackets expresses this), so if we simply substitute the values stored in the computer memory for the TF/SF respectively, as denoted, the equality will no longer hold. In order to make eq. (3.35) consistent, one must subtract the incident field from the total field where appropriate. Mathematically, it means that the scattered field in this point satisfies eq. (3.31), due to linearity. Programmatically, this can be done as a separate step:

$$H_y|_{i_l-1/2,j}^{n+1/2} := H_y|_{i_l-1/2,j}^{n+1/2} - \frac{\Delta t}{\Delta x} E_{z,in}|_{i_l,j}^{n}, \tag{3.36}$$

where $E_{z,in}$ is the incident electric field (accordingly, $H_{x,in}$ and $H_{y,in}$ correspond with the incident magnetic field). Equation (3.36) and others of its kind should be understood the following way: the value for H_y in the specified point is first computed according to eq. (3.31), corrected as per the right-hand side of eq. (3.36), and then the new value is assigned to H_y. We denote the assignment operator as := here to distinguish it from the equality sign, although programming languages such as Fortran use = for the assignment operator.

Analogously, for the electric field one obtains:

$$E_z|_{i_l,j}^{n+1} := E_z|_{i_l,j}^{n+1} - \frac{\Delta t}{\Delta x} H_{z,in}|_{i_l-1/2,j}^{n+1/2}. \tag{3.37}$$

In the same manner, we write for the right boundary located at i_r:

$$H_y|_{i_r+1/2,j}^{n+1/2} := H_y|_{i_r+1/2,j}^{n+1/2} - \frac{\Delta t}{\Delta x} E_{z,in}|_{i_r,j}^{n}, \tag{3.38}$$

$$E_z|_{i_r,j}^{n+1} := E_z|_{i_r,j}^{n+1} - \frac{\Delta t}{\Delta x} H_{y,in}|_{i_r+1/2,j}^{n+1/2}; \tag{3.39}$$

for the top boundary at j_t:

$$H_x|_{i,j_t+1/2}^{n+1/2} := H_x|_{i,j_t+1/2}^{n+1/2} - \frac{\Delta t}{\Delta y} E_{z,in}|_{i,j_t}^{n}, \tag{3.40}$$

$$E_z|_{i,j_t}^{n+1} := E_z|_{i,j_t}^{n+1} - \frac{\Delta t}{\Delta y} H_{x,in}|_{i,j_t+1/2}^{n+1/2}; \tag{3.41}$$

for the bottom boundary at j_b:

$$H_x|_{i,j_b-1/2}^{n+1/2} := H_x|_{i,j_b-1/2}^{n+1/2} + \frac{\Delta t}{\Delta y} E_{z,in}|_{i,j_b}^{n}, \tag{3.42}$$

$$E_z|^{n+1}_{i,j_b} := E_z|^{n+1}_{i,j_b} + \frac{\Delta t}{\Delta y} H_{x,in}|^{n+1/2}_{i,j_b-1/2}. \tag{3.43}$$

There is an important nuance, however: simply substituting the analytical values of the source field on the Huygens surface will result in spurious field leaks outside the TF/SF boundary. This is due to the mismatch between analytical and numerical dispersion. In order to address this issue, propagation of the source field must be computed in such a way that its dispersion is the same (or at least close enough) as the numerical dispersion of the FDTD scheme. One of the most effective solutions to that problem was proposed by Tan and Potter [38, 39] (an expanded description can also be found in a computational textbook by Taflove *et al* [40]). For rational incidence angles of the source plane wave, such that

$$\tan \phi_r \equiv \frac{p_y}{p_x} = \frac{m_y \Delta x}{m_x \Delta y}$$

and

$$\tan \theta_r \equiv \frac{\sqrt{p_x^2 + p_y^2}}{p_z} = \frac{\sqrt{m_x^2/\Delta x^2 + m_y^2/\Delta y^2}}{m_z/\Delta z},$$

where m_x, m_y and m_z are integers and $\mathbf{p}$ is a unit vector pointing in the propagation direction, it is possible to construct an auxiliary one-dimensional source grid in such a way that its dispersion is perfectly matched with the main two- or three-dimensional grid. Moreover, the discretised field values from the source grid can be directly mapped onto the main grid in a straightforward manner. This allows to handle the TF/SF boundary with machine precision.

Using this approach, the propagation of a plane-wave pulse[4] in vacuum, presented at fig. 3.3, has been computed in order to test the method. Since there is no scattering object, the scattered field should be zero. The field leaked through the TF/SF boundary, i.e. the numerical error, is within the limits of machine precision (fig. 3.4).

The auxiliary 1D grid in this implementation can be terminated with its own absorbing boundary condition (which we shall discuss in detail in the following subsection), so that continuous plane waves can be introduced.

3.2.2 Perfectly Matched Layer absorbing boundary conditions for time-dependent metamaterials

The proper choice of boundary conditions is important for numerical simulations. Sometimes they are imposed by the nature of the problem studied: perfect electric or magnetic conductors (PEC/PMC), periodicity, etc are all good examples of that. However, open boundaries are often needed, and in order to describe them, appropriate conditions must satisfy two requirements: firstly, they should be non-reflective for all incidence angles; secondly, they should ensure that the radiation vanishes somehow (fig. 3.5), so that the grid can be terminated, for example, with a PEC.

[4] One usually refers to *pulses* when the electromagnetic radiation is confined in time (as opposed to a sinusoidal wave, for example) and to *beams* when it is confined in space. 'Compact' electromagnetic waves, confined both in space and time, are sometimes referred to as 'light bullets'.

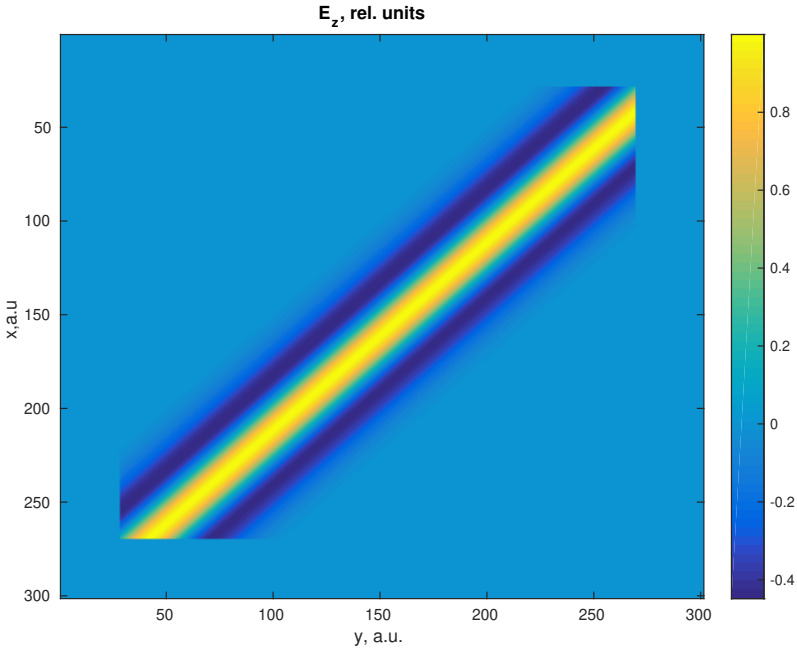

Figure 3.3: *A momentary 'snapshot' of the normalised electric field for a plane-wave pulse introduced into the computational domain via a TF/SF technique. The pulse is propagating from the upper-left corner at the angle of 45°, and the spatial distribution of the field is shown. One can observe that the field is present only in the TF area (in the middle), since the scattered field is zero in the absence of a scattering object.*

These conditions have not yet been realised generally on a thin boundary, however, it can be done for a finite area adjacent to the outer boundary of the computational grid. In such a configuration, the inner boundary of the auxiliary layer, matched to the actual computational domain, is reflectionless, and the field decays within the layer until it reaches effectively zero at the outer boundary. This is realised in a common state-of-the-art solution to the problem — so-called Perfectly Matched Layer (PML) (discussing other types of absorbing boundary conditions is outside the scope of this work; a comprehensive review can be found in literature [37, 41]). There are several variations of the PML available, such as Berenger's original split-field formulation [42], uniaxial PML (UPML) [43], convolutional PML (CPML) [44] and a variation thereof referred to as nearly perfectly matched layer (NPML) [45]. In our study CPML in particular is used, since it is well suited for time-dependent media. Let us discuss the main ideas of PML in general, the choice and advantages of CPML for time-dependent media in particular and its implementation for FDTD in detail.

There are two ways to reach the goal of PML. The first possibility is to leave Maxwell's equations within the PML intact and obtain the requisite properties by selecting an appropriate mathematical model of the medium. This is realised in the UPML, where a fictitious uniaxial dielectric is introduced within the PML. The second possibility is to

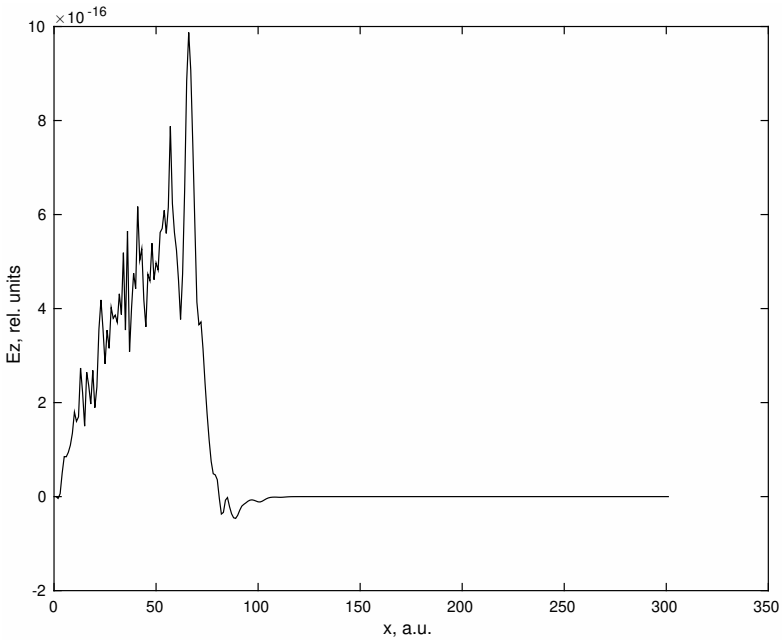

Figure 3.4: *Spatial distribution (x coordinate) of the electric field (normalised by the peak value of the incident field) leaked through the TF/SF boundary into the SF area (see fig. 3.3).*

modify the equations themselves in such a way that they are compatible with Maxwell's equations on the outer boundary of the PML, resulting in no reflection, and they ensure the field decay with the actual PML. Such modifications can be formulated or interpreted in terms of a variable change, or 'coordinate stretch'. Each coordinate, e.g. x, is mapped onto the complex coordinate, e.g. x' (in this sense, the UPML is a stretch of fields rather than coordinates). The new equations are then obtained in frequency domain by replacing the coordinates x, y, z with x', y', z'.

The coordinate stretch can be incorporated in time domain on either the left-hand side of eqs. (3.27)–(3.29) or the right-hand side. The former corresponds with the split-field formulation, while the latter — with CPML. It is remarkable that the second possibility modifies only the spatial part of the curl equations regardless of the material properties, meaning that the generalisation of the method for the time-dependent media is straightforward, similar to other general media (e.g. lossy, anisotropic, nonlinear, etc) [41, 44]. This means that the CPML formulation is suitable for our study of time-dependent metamaterials.

Let us quickly recap the general ideas of CPML. Firstly, the coordinate stretch is analytically derived in frequency domain (ω instead of t) using the following transformation:

$$x' = \int_0^x s_x(\xi, \omega) d\xi, \quad y' = \int_0^y s_y(\xi, \omega) d\xi, \quad z' = \int_0^z s_z(\xi, \omega) d\xi, \tag{3.44}$$

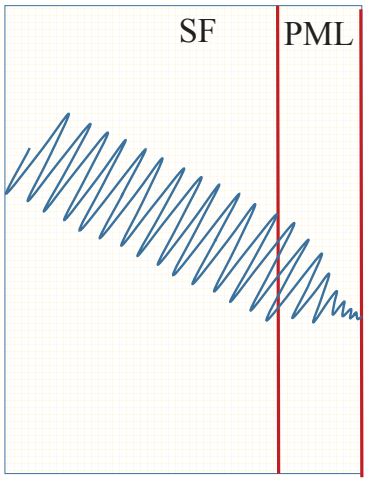

Figure 3.5: *A PML absorbing a wave impinging on the boundary*

so that eqs. (3.27)–(3.29) read as:

$$i\omega\tilde{B}_x = -\frac{\partial\tilde{E}_z}{\partial y'} = -\frac{1}{s_y}\frac{\partial\tilde{E}_z}{\partial y}, \tag{3.45}$$

$$i\omega\tilde{B}_y = \frac{\partial\tilde{E}_z}{\partial x'} = \frac{1}{s_x}\frac{\partial\tilde{E}_z}{\partial x}, \tag{3.46}$$

$$i\omega\tilde{D}_z = \frac{\partial\tilde{H}_y}{\partial x'} - \frac{\partial\tilde{H}_x}{\partial y'} = \frac{1}{s_x}\frac{\partial\tilde{H}_y}{\partial x} - \frac{1}{s_y}\frac{\partial\tilde{H}_x}{\partial y} \tag{3.47}$$

where tilde denotes the frequency domain.

The stretching coefficients are either taken in the traditional form, which is implemented in this work:

$$s_w = 1 + \frac{\sigma_w(\xi)}{i\omega}, \tag{3.48}$$

where $w = x, y, z$, or the more general complex frequency-shifted [46] coefficient is used:

$$s_w = \kappa_w(\xi) + \frac{\sigma_w(\xi)}{\alpha_w(\xi) + i\omega}. \tag{3.49}$$

The second form is generally useful for moving away the frequency pole in eq. (3.48), i.e. improving the low-frequency regime, and for applications involving evanescent waves in particular; although the numerical scheme presented above (eqs. (3.30)–(3.32)) supports

it, as would the already written code with minimal modifications[5], we do not use it in this work.

The condition for the absence of reflection is that the PML medium is stretched only in the direction perpendicular to the surface. For example, in a 2D case $\sigma_x \neq 0,\ \sigma_y = 0$ near the left boundary $x = 0$ and $\sigma_x = 0,\ \sigma_y \neq 0$ near the lower boundary $y = 0$ (in the corner, these areas overlap, so that $\sigma_x \neq 0,\ \sigma_y \neq 0$). One can show that a propagating (homogeneous) plane wave with a real wavevector $\mathbf{k} = \{\omega \cos\theta, \omega \sin\theta\}$

$$u = \exp(i\omega t - i\omega \sin\theta y - i\omega \cos\theta x), \tag{3.50}$$

impinging on the boundary $x = 0$, is transmitted (assuming that $\sigma_w(\xi)$ is constant[6]) into an attenuated wave with a complex wavevector component in the direction of the stretch if the stretching factor (3.48) is chosen:

$$u = \exp(i\omega t - i\omega \sin\theta y - i\omega \cos\theta x) \exp(-\sigma_x \cos\theta x).$$

Attenuation of evanescent waves with the more general complex frequency-shifted stretching factor (3.49) can also be analysed [37, 41].

Secondly, coordinate transformation (3.44) with stretching factor (3.48) or (3.49) must be implemented in time domain:

$$\frac{\partial B_x}{\partial t} = -\overline{s_y}(t) * \frac{\partial E_z}{\partial y}, \tag{3.51}$$

$$\frac{\partial B_y}{\partial t} = \overline{s_x}(t) * \frac{\partial E_z}{\partial x}, \tag{3.52}$$

$$\frac{\partial D_z}{\partial t} = \overline{s_x}(t) * \frac{\partial H_y}{\partial x} - \overline{s_y}(t) * \frac{\partial H_x}{\partial y}, \tag{3.53}$$

where the asterisk denotes a convolution operator and $\overline{s_w}$ is the inverse Fourier transform of the inverse of the stretching factor s_w:

$$\overline{s_w}(t) = \frac{\delta(t)}{\kappa_w} + \zeta_w(t),$$

$$\zeta_w(t) = -\frac{\sigma_w}{\kappa_w^2} \exp\left[\left(-\frac{\sigma_w}{\kappa_w} + \alpha_w\right) t\right] u(t),$$

and $u(t)$ is the unit step function.

Now, for example, eq. (3.52) can be written as:

$$\frac{\partial B_y}{\partial t} = \frac{1}{\kappa_x} \frac{\partial E_z}{\partial x} + \psi_{Ez,x}, \tag{3.54}$$

[5]The factors $\kappa_w(\xi)$ in particular should be implemented in the field update equations (see below) in an optimal way, which would require some loop splitting. In the current version of the code, $\kappa \equiv 1$ is assumed everywhere, so it is not necessary.

[6]In a realistic numerical simulation, $\sigma_w(\xi)$ is scaled, which can be essentially considered as a multilayered PML with piecewise-constant σ. Due to this, our conclusions about PML's properties remain generally true.

where

$$\psi_{Ez,x} = \zeta_x * \frac{\partial E_z}{\partial x}. \tag{3.55}$$

Generally, computing this would require cumbersome calculations of the convolutions, making it impractical for numerical simulations. However, due to the the choise of stretching coefficients (3.49), the additional convolution terms like (3.55) can be evaluated recursively [37, 41], resulting in an excellently efficient scheme:

$$\psi_{Ez,x}|^{n+1/2}_{i+1/2,j} = b_x \psi_{Ez,x}|^{n-1/2}_{i+1/2,j} + c_x \frac{\Delta E_z|^n_{i+1/2,j}}{\Delta x}, \tag{3.56}$$

where ΔE_z is the central difference in space:

$$\Delta E_z|^n_{i+1/2,j} = E_z|^n_{i+1,j} - E_z|^n_{i,j},$$

and

$$b_x = \exp\left[\left(-\frac{\sigma_x}{\kappa_x} + \alpha_x\right)\Delta t\right],$$
$$c_x = \frac{\sigma_x}{\kappa_x(\sigma_x + \kappa_x \alpha_x)}(b_x - 1).$$

Notice that the electric field in eq. (3.56) is not evaluated at the proper moment of time, however, this approximation provides results good enough from a practical point of view, meaning that its accuracy is generally sufficient for applications of the CPML, according to Taflove *et al* [37]. Convolutional terms for other field components in eqs. (3.51)–(3.53) are introduced completely analogously.

In order to minimise spurious numerical reflections, $\sigma_w(\xi)$ is scaled from zero in the inner boundary's vicinity to the maximum value (which can be estimated with respect to the reflection coefficient desired) at the outer boundary, usually as a polynomial function or a geometric progression.

The reflection of a so-called Ricker pulse from a PML matched to a time-dependent medium is presented in Paper 1. The reflected 'amplitude' (normalised by the peak value, or the 'amplitude', of the incident pulse) in this case is the order of 10^{-6}, demonstrating good applicability of CPML to the problems put forth in this work.

3.3 Computer implementation

Depending on the size of the numerical problem to be solved, the computational burden can be significant. Therefore, it is desirable for the implementation to be efficient.

As it is often the case with finite-difference schemes, the problem is memory-bound, i.e. performance is limited by memory access (as one can see from eqs. (3.30)–(3.32), both the storage and numeric operations have the complexity of $O(N^2)$). This implies that efficient handling of memory, locality and good cache use are determining factors.

Another important practical aspect is the choice of programming language suited for numerical calculations. In this work, Fortran 90 is used for the computational part.

With all those factors considered, we have found that with modern optimising compilers, such as GCC (to a lesser extent, Intel compiler was also tested), it hard to improve on their performance; moreover, some of our attempts to improve memory locality 'manually' by blocking resulted in a significant overall performance decrease and rather suboptimal L1 cache use, as demonstrated by profiling. Therefore we conclude that it might be more important for practical purposed to use an efficient optimising compiler with proper options; nested loop optimisation is particularly important for the FDTD scheme.

Finally, the issue of storing the values of ϵ and μ requires special attention. For time-dependent media in particular the values of material parameters at each point are stored for two time layers, as follows from eqs. (3.30)–(3.32). This means, generally speaking, that roughly two third of all allocated memory is used for describing media properties. In a very special case where there is only a small number of discrete material blocks constituting the system in question, the amount of storage required can be greatly reduced by using integer 'pointers' to the medium type; for example, on a 64-bit machine for calculations in double precision, the overall reduction is approximately eight times for one-byte integers. However, this can require more careful programming [37] and is a potential development area for our implementation.

4 Summary, conclusion and outlook

4.1 Main results

The central result of this thesis, summarised in Paper 1, is the development and implementation of a powerful numerical method for simulating time-dependent electromagnetic media. Since popular existing FDTD software supports simulating only time-invariant media, the code developed is distinct in the sense that it provides us with a tool for solving electromagnetic problems in time-dependent materials. We have applied it to study transmission of plane electromagnetic waves through a slab with the dielectric permittivity and magnetic permeability being linear functions of time.

Incident electromagnetic radiation is introduced into the computational domain via the total-field / scattered-field (TF/SF) source condition in the so-called discrete-planewave formulation. We have practically tested that, unlike the 'naive' implementation of the TF/SF technique, the computational error introduced is within the limits of computational precision, meaning that no spurious field leaks across the TF/SF boundary occur.

A convolutional perfectly matched layer (CPML) is used as an absorbing boundary condition. In Paper 1 we have numerically demonstrated that it is suitable for time-dependent materials, since the level of numerical reflection from a CPML matched to a time-dependent metamaterial slab corresponds with the state-of-the-art results.

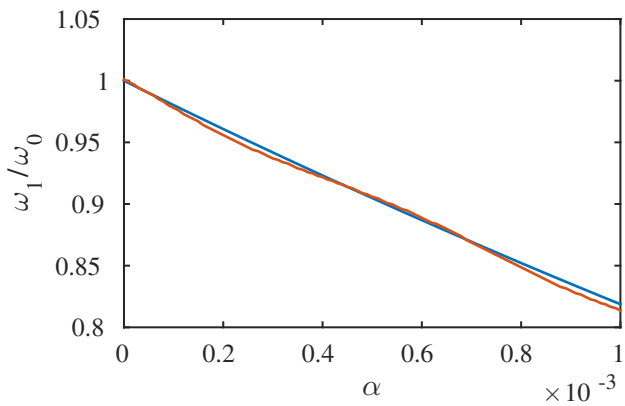

Figure 4.1: *Analytical (blue) and numerical (red) dependences of the transmitted wave's relative frequency shift on the modulation rate α of the metamaterial slab's dielectric permittivity and magnetic permeability*

Transmission of both monochromatic waves and finite pulses through a time-dependent metamaterial slab with $\epsilon(t) = \mu(t) = 1 + \alpha(t - t_0)$ (where α and t_0 are the parameters of the model), has been analysed. The numerical results for monochromatic waves are in agreement (see fig. 4.1) with the theoretical formula obtained in an earlier work by Ginis *et al* [47], and thus the code is benchmarked and shown to produce valid results. The spectral shift between incident and transmitted waves computed numerically (fig. 4.2) matches the

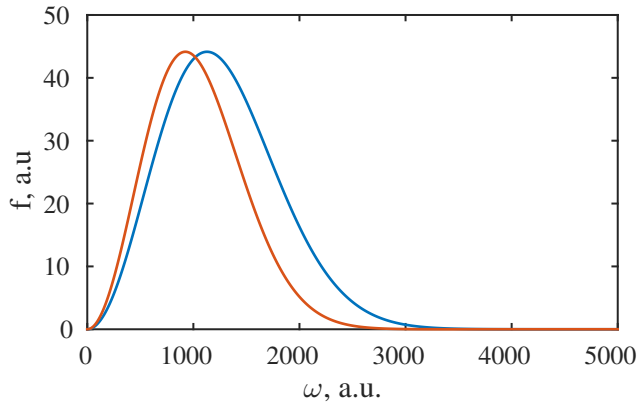

Figure 4.2: *Spectra of the incident (blue) and transmitted (red) pulses, computed numerically.*

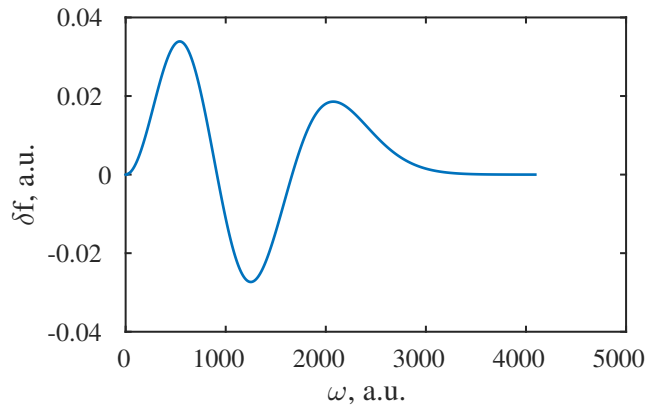

Figure 4.3: *The difference between the spectral density $f(\omega)$ of the transmitted pulse (see above) computed analytically and numerically (fig. 4.2). The results obtained with both methods are in good agreement.*

result derived analytically in Paper 1 as well (fig. 4.3). We have also demonstrated how the effect in question could be used to switch optical pulses between frequency channels in a wavelength-division multiplexer. This is a proof-of-concept example of how the code can be applied.

4.2 Discussion

The technique developed within the context of this work is the first — and probably the most difficult — step to broadening our understanding of time-dependent optical materials. There are two major directions in which it could be further applied.

Firstly, metamaterials with certain macroscopic properties are generally designed for a particular purpose, namely for some optical phenomena occurring in them. Therefore, simulating macroscopic models describing effective media with certain time-dependent parameters is important in order to determine the effects that such metamaterials can exhibit.

Secondly, the same tool and technique is also applicable, albeit at a different level, to designing new metamaterials, for the definitions of 'macroscopic' and 'microscopic' are relative, and the building blocks — meta-atoms — can be considered as macroscopic structures on a different scale. For example, 'microscopic' (meaning that they are much smaller than the characteristic wavelength) wires and resonators, in turn, consist of 'macroscopic' blocks, e.g. pieces of dielectric, metal etc with macroscopic properties such as dielectric permittivity, conductivity and so on, which could be simulated with the numerical method presented here.

To sum up, this work and its results could be applied to investigate the properties of time-dependent metamaterial models and to help answer the question how such metamaterials can be constructed.

References

[1] M. Lapine and S. Tretyakov. Contemporary notes on metamaterials. *IET Microwaves, Antennas Propagation* **1**.1 (2007), 3–11.

[2] V. G. Veselago. The electrodynamics of substances with simultaneously negative values of ϵ and μ. *Soviet Physics Uspekhi* **10**.4 (1968), 509.

[3] L. Mandelstam. *Complete Works. 5 volumes.* Izd. AN SSSR Moscow, 1947.

[4] D. Sivukhin. The energy of electromagnetic waves in dispersive media. *Opt. Spektrosk.* **3** (1957), 308–312.

[5] V. Pafomov. Transition radiation and Cerenkov radiation. *Soviet. Phys. JETP* **9** (1959), 1321–1324.

[6] M. Notomi. Theory of light propagation in strongly modulated photonic crystals: Refractionlike behavior in the vicinity of the photonic band gap. *Phys. Rev. B* **62** (16 2000), 10696–10705.

[7] V. A. Podolskiy and E. E. Narimanov. Strongly anisotropic waveguide as a nonmagnetic left-handed system. *Phys. Rev. B* **71** (20 2005), 201101.

[8] L. D. Landau, E. Lifshitz, and L. Pitaevskii. *Electrodynamics of continuous media.* Vol. 8. Pergamon Press, 2013.

[9] D. R. Smith et al. Composite Medium with Simultaneously Negative Permeability and Permittivity. *Phys. Rev. Lett.* **84** (18 2000), 4184–4187.

[10] R. A. Shelby, D. R. Smith, and S. Schultz. Experimental Verification of a Negative Index of Refraction. *Science* **292**.5514 (2001), 77–79.

[11] J. Brown. Artificial dielectrics. *Prog. Dielectr.* **2** (1960), 195–225.

[12] D. R. Smith and N. Kroll. Negative Refractive Index in Left-Handed Materials. *Phys. Rev. Lett.* **85** (14 2000), 2933–2936.

[13] S. I. Maslovski, S. A. Tretyakov, and P. A. Belov. Wire media with negative effective permittivity: A quasi-static model. *Microwave and Optical Technology Letters* **35**.1 (2002), 47–51.

[14] J. B. Pendry et al. Magnetism from conductors and enhanced nonlinear phenomena. *IEEE Transactions on Microwave Theory and Techniques* **47**.11 (1999), 2075–2084.

[15] F. Martín and J. Bonache. Application of RF-MEMS-Based Split Ring Resonators (SRRs) to the Implementation of Reconfigurable Stopband Filters: A Review. *Sensors* **14**.12 (2014), 22848–22863.

[16] V. M. Shalaev. Optical negative-index metamaterials. *Nature photonics* **1**.1 (2007), 41–48.

[17] C. M. Soukoulis and M. Wegener. Past achievements and future challenges in the development of three-dimensional photonic metamaterials. *Nature Photonics* **5**.9 (2011), 523–530.

[18] J. B. Pendry. Negative Refraction Makes a Perfect Lens. *Phys. Rev. Lett.* **85** (18 2000), 3966–3969.

[19] N. Engheta and R. W. Ziolkowski. *Metamaterials: physics and engineering explorations.* John Wiley & Sons, 2006.

[20] N. Engheta. Circuits with Light at Nanoscales: Optical Nanocircuits Inspired by Metamaterials. *Science* **317**.5845 (2007), 1698–1702.

[21] N. Engheta. From RF Circuits to Optical Nanocircuits. *IEEE Microwave Magazine* **13**.4 (2012), 100–113.
[22] E. Shamonina and L. Solymar. Properties of magnetically coupled metamaterial elements. *Journal of Magnetism and Magnetic Materials* **300**.1 (2006). The third Moscow International Symposium on Magnetism 2005, 38–43.
[23] N. Yu and F. Capasso. Flat optics with designer metasurfaces. *Nature materials* **13**.2 (2014), 139–150.
[24] E. Martini et al. Flat Optics for Surface Waves. *IEEE Transactions on Antennas and Propagation* **64**.1 (2016), 155–166.
[25] A. Vakil and N. Engheta. Transformation Optics Using Graphene. *Science* **332**.6035 (2011), 1291–1294.
[26] A. Vakil and N. Engheta. Fourier optics on graphene. *Phys. Rev. B* **85** (7 2012), 075434.
[27] A. Boardman et al. Active and tunable metamaterials. *Laser & Photonics Reviews* **5**.2 (2011), 287–307.
[28] J. P. Turpin et al. Reconfigurable and tunable metamaterials: a review of the theory and applications. *International Journal of Antennas and Propagation* **2014** (2014).
[29] A. Q. Liu et al. Micromachined tunable metamaterials: a review. *Journal of Optics* **14**.11 (2012), 114009.
[30] N.-H. Shen et al. Broadband blueshift tunable metamaterials and dual-band switches. *Phys. Rev. B* **79** (16 2009), 161102.
[31] M. Kafesaki et al. Optically switchable and tunable terahertz metamaterials through photoconductivity. *Journal of Optics* **14**.11 (2012), 114008.
[32] Y. Fan et al. Tunable terahertz meta-surface with graphene cut-wires. *ACS Photonics* **2**.1 (2015), 151–156.
[33] V. Ginis et al. Tunable terahertz frequency comb generation using time-dependent graphene sheets. *Phys. Rev. B* **91** (16 2015), 161403.
[34] K. Yee. Numerical solution of initial boundary value problems involving Maxwell's equations in isotropic media. *IEEE Transactions on Antennas and Propagation* **14**.3 (1966), 302–307.
[35] I. Lindell. *Electromagnetic Waves in Chiral and Bi-isotropic Media*. Antennas and Propagation Library. Artech House, 1994.
[36] A. Serdyukov et al. *Electromagnetics of bi-anisotropic materials: Theory and applications*. Gordon and Breach Science Publishers, 2001.
[37] A. Taflove and S. Hagness. *Computational Electrodynamics: The Finite-difference Time-domain Method*. Artech House antennas and propagation library. Artech House, 2005.
[38] T. Tan and M. Potter. 1-D Multipoint Auxiliary Source Propagator for the Total-Field/Scattered-Field FDTD Formulation. *IEEE Antennas and Wireless Propagation Letters* **6** (2007), 144–148.
[39] T. Tan and M. Potter. FDTD Discrete Planewave (FDTD-DPW) Formulation for a Perfectly Matched Source in TFSF Simulations. *IEEE Transactions on Antennas and Propagation* **58**.8 (2010), 2641–2648.
[40] A. Taflove, A. Oskooi, and S. G. Johnson. *Advances in FDTD computational electrodynamics: photonics and nanotechnology*. Artech house, 2013.

[41] J. Bérenger. *Perfectly Matched Layer (PML) for Computational Electromagnetics*. Synthesis lectures on computational electromagnetics. Morgan & Claypool Publishers, 2007.

[42] J.-P. Berenger. A perfectly matched layer for the absorption of electromagnetic waves. *Journal of Computational Physics* **114**.2 (1994), 185–200.

[43] Z. S. Sacks et al. A perfectly matched anisotropic absorber for use as an absorbing boundary condition. *IEEE Transactions on Antennas and Propagation* **43**.12 (1995), 1460–1463.

[44] J. A. Roden and S. D. Gedney. Convolutional PML (CPML): An efficient FDTD implementation of the CFS-PML for arbitrary media. *Microwave and optical technology letters* **27**.5 (2000), 334–338.

[45] S. A. Cummer. A simple, nearly perfectly matched layer for general electromagnetic media. *IEEE Microwave and Wireless Components Letters* **13**.3 (2003), 128–130.

[46] M. Kuzuoglu and R. Mittra. Frequency dependence of the constitutive parameters of causal perfectly matched anisotropic absorbers. *IEEE Microwave and Guided Wave Letters* **6**.12 (1996), 447–449.

[47] V. Ginis et al. Frequency converter implementing an optical analogue of the cosmological redshift. *Opt. Express* **18**.5 (2010), 5350–5355.